Electrochemically assisted photocatalytic degradation of contaminants of emerging concern in simulated wastewater using WO3 – Elucidation of mechanisms

Title: Electrochemically assisted photocatalytic degradation of contaminants of emerging concern in simulated wastewater using WO_3 – Elucidation of mechanisms

Authors: A. Tolosana-Moranchel[a,b*], S. McMichael[a], J.W.J. Hamilton[a], J.A. Byrne[a], P. Fernández-Ibañez[a]

[a]Nanotechnology and Integrated BioEngineering Centre, School of Engineering, Ulster University, Northern Ireland, BT37 0QB, United Kingdom

[b]Grupo de Energía y Química Sostenibles, Instituto de Catálisis y Petroleoquímica, CSIC. Marie Curie 2, 28049, Madrid, Spain

* Corresponding author:

Alvaro Tolosana Moranchel: alvaro.tolosana@csic.es Pilar Fernandez Ibanez: p.fernandez@ulster.ac.uk

ABSTRACT

In this work, the performance of a photoelectrochemical cell to degrade a mixture of contaminants of emerging concern (CECs) in distilled water and simulated wastewater effluents (SWWE) was assessed. The CECs mixture included trimethoprim (TMP), diclofenac (DFC), sulfamethoxazole (SMX) and carbamazepine (CBZ) (100 $\mu g \cdot L^{-1}$ each). WO_3 nanoplate-like structures synthesized on fluorine tin oxide coated glass (FTO) were used as the photoanode with Pt or carbon gas diffusion electrodes (GDE) as the counter electrode. The most efficient degradation of the CECs was obtained with the WO_3-GDE combination. Significant degradation of the CECs was observed under visible only radiation. Even under visible radiation, reasonable rate constants $5.67 \cdot 10^{-3}$, $5.35 \cdot 10^{-3}$, $2.9 \cdot 10^{-3}$ and $4.35 \cdot 10^{-3}$ min^{-1} were obtained for TMP, SMX, CBZ and DFC degradation. The degradation mechanism at the cathode and the photoanode was elucidated using a two-compartment cell, which allowed the identification of reactive species generated at each electrode. Photogenerated holes were the main responsible for CEC degradation in SWWE. With the carbon GDE, a high Faradaic efficiency (55%) for H_2O_2 production was observed.

Keywords: WO_3 photoanode, photoelectrocatalysis, carbon gas diffusion electrode, contaminant of emerging concern, reactive oxygen species

1. **Introduction**

There is global concern about the pollution of water resources with contaminants of emerging concern (CECs) due to their potential threat for the environment and human health [1,2]. Pharmaceuticals residues have been detected in environmental water bodies at concentrations ranging from $ng \cdot L^{-1}$ to $\mu g \cdot L^{-1}$ [3]. They can pose a serious threat to human and lead to toxic effects [1,3–5]. Conventional wastewater treatment plants are not able to effectively remove CECs, and more advanced treatment processes must be developed to address this challenge.

Advanced Oxidation Processes (AOPs) are a potential solution for the degradation of CECs in water [6]. Heterogeneous photocatalysis generates reactive oxygen species (ROS) and can degrade refractory pollutants, including CECs, and inactivate disinfection resistant waterborne microorganisms [7]. When a semiconductor photocatalyst is irradiated by photons with energy equal or greater than the band gap energy, charge carriers are generated. Valence band holes (h^+) can either directly oxidize the organic compound or oxidise water to generate hydroxyl radicals ($HO^{\cdot}$) that will attack organic matter [8]. If the conduction band edge potential is negative enough (as with TiO_2) photogenerated electrons (e^-) can reduce O_2 to produce superoxide radical anion and hydrogen peroxide. Photocatalysis can be inefficient due to fast recombination of charge carriers. Photoelectrocatalysis (also referred to as electrochemically assisted photocatalysis (EAP) uses a photo-electro-chemical cell with an applied potential that helps separate charge carriers thus reducing the rate of recombination and increasing the efficiency of electron and hole transfer to solution [8]. The use of an electrically biased counter electrode means that photogenerated electrons can be transferred to solution even when the photoanode does not have a negative enough conduction band edge potential. The most commonly studied photocatalyst is TiO_2 but it can only absorb UV radiation, hence limiting the solar efficiency [9]. There is much interest in photocatalysts with a narrower band gap energy which can utilise visible photons and improve the solar efficiency [10]. WO_3 has good chemical resistance and is able to utilise visible photons up to 470 nm [11]. In addition, nano-engineering of photocatalysts to give TiO_2 nanotubes [12,13] and WO_3 nanoplates [11,14], has

been reported to result in improved photocurrents and greater photocatalytic activity due to exposed reactive facets and shorter charge diffusion lengths [15]. Pt is commonly used as the counter electrode material in electrochemically assisted photocatalysis studies [10], however, other less expensive and earth abundant materials can be used. For example carbon gas diffusion electrodes made from carbon or graphite felts, carbon-PTFE GDEs and carbon sponge [16], have shown good performance because they favour the generation of H_2O_2 by the 2 electron reduction of molecular oxygen and provide good stability, conductivity and chemical resistance [17,18].

Most reported studies relating to the degradation of CECs will focus on only one compound [19,20] but in real applications there will most likely be mixtures of several CECs and the evaluation of electrochemically assisted photocatalysis for the degradation of a mixture of CECs, at realistic concentrations, is therefore of interest [17,18]. Only a few studies have reported results of electrochemically assisted photocatalysis for wastewater treatment [21–24] using concentrations of $mg \cdot L^{-1}$, which are well above realistic levels [10]. The configuration of the cell will have significant influence on the performance of the system [25]. A front-side configuration can only be used if the photocatalyst is coated on non-transparent substrates, for example irradiating through a mesh [26]. Thus, the radiation intensity will drop upon travelling through the solution due to its absorption by the electrolyte and other chemical compounds. In the case of wastewater which may absorb strongly in the same wavelength range as the photocatalyst, the design of thin-layer or rotating disk EAP reactors have been identified as an option to minimise absorption losses [25,27,28]. Alternatively, optically transparent supporting electrodes (OTE) are often used, including Fluorine doped Tin Oxide (FTO) or Indium doped Tin Oxide (ITO); in this case they allow back-face irradiation. Moreover, if the photoanode is irradiated back-face, a flat plate/sandwich configuration can be used in which the photoanode faces towards the cathode, leading to a more uniform current density distribution and lower cell resistance [29].This study aims at evaluating the performance of a cell with back-face irradiated photoanode to degrade a mixture of CECs, in a realistic range of few $\mu g \cdot L^{-1}$, in simulated wastewater effluent (SWWE). WO_3 nanoplates electrodes were selected as the photoanode as they show good performance

even under visible only irradiation as compared to TiO_2 [11]. The degradation rates obtained employing Pt and carbon paper (CP), a gas diffusion electrode (GDE), as the counter electrode were compared. A careful examination was carried out using scavengers and a two-compartment cell to determine which oxidizing species are the most important and at which electrode they were generated. To the best of our knowledge, no studies have been published reporting a thorough study of the different ROS produced in simulated wastewater effluent using a EAP cell with a WO_3 photoanode and carbon GDE cathode.

2. Experimental section

2.1. Materials

All the chemicals used in this study were analytical grade and used as received. Methanol (HPLC grade, CH_3OH>99.9%), FTO glass (Sigma-Aldrich, fluorine-doped tin oxide SnO_2:F ~7 Ω/sq), SU8 photoresist (Microchem), hydrochloric acid (Merk, HCl 37%), sodium tungstate dehydrate (Sigma-Aldrich, $Na_2WO_4 \cdot 2H_2O$>99%), Acetonitrile (Sigma-Aldrich, CH_3CN>99.9%), sodium oxalate (Aldrich, $Na_2C_2O_4$>99.5%), Decon™ Decon 90 (Decon Laboratories Ltd.), sodium sulfite (ACS reagent, Na_2SO_3≥98.0%), potassium iodide (Sigma Aldrich, KI ≥99.0%), hydroquinone (Sigma-Aldrich, $C_6H_6O_2$≥99.0%), formic acid (Merk, HCOOH>98%), p-benzoquinone (reagent grade, $C_6H_4O_2$≥98%), isopropanol (C_3H_8O≥99.9%), coumarin (Sigma-Aldrich, HPLC grade, $C_9H_6O_2$≥99.0%), umbelliferone (Sigma-Aldrich, $C_9H_6O_3$≥98.0%), sodium sulfate (Sigma-Aldrich, Na_2SO_4>99%), hydrogen peroxide (Sigma-Aldrich, H_2O_2≥30%, for trace analysis), titanium oxysulfate in dilute sulfuric acid (Sigma-Aldrich $TiOSO_4$, 27-31% H_2SO_4 basis), trimethoprim (Merck HPLC grade, $C_{14}H_{18}N_4O_3$≥98%), diclofenac sodium salt (Merck, $C_{14}H_{10}Cl_2NNaO_2$≥98%), sulfamethoxazole (Merck, $C_{10}H_{11}N_3O_3S$ analytical standard), carbamazepine (Merck $C_{15}H_{12}N_2O$), $NaHCO_3$ (Sigma-Aldrich, ≥99.7%), $CaSO_4.2H_2O$ (Sigma-Aldrich, ≥99%), peptone (Sigma-Aldrich), $MgSO_4$ (Sigma-Aldrich, ≥99.5%), NaCl (Sigma-Aldrich, ≥99%), KCl (Sigma-Aldrich, ≥99%), beef extract (Sigma-Aldrich), humic acid (Sigma-Aldrich, technical grade), tannic acid (Sigma-Aldrich, ACS reagent), lignosulfonic acid sodium salt (Sigma-Aldrich, average M_w ~52,000,

168 average M_n ~7,000), sodium lauryl sulfate (Sigma-Aldrich, United States
169 Pharmacopeia (USP) Reference Standard), gum arabic from acacia tree (Sigma-
170 Aldrich, spray dried), $(NH_4)_2SO_4$ (Sigma-Aldrich, ≥99%) and K_2HPO_4
171 (Sigma-Aldrich, ≥98%). All the solutions were prepared with deionized water (15
172 $M\Omega \cdot cm^{-1}$).

173

174 *2.2. Preparation of WO_3 photoanode*

175

176 WO_3 structures were grown hydrothermally on FTO glass coupons of, 8.4 cm x
177 8.4 cm used in the one-compartment cell (Figure S1) and 2 cm x 1.5 cm for the
178 two-compartment cell (Figure S2), as previously reported [11]. A full description
179 of the synthesis methodology can be found in the supplementary information. A
180 thorough characterization of the material tested here was carried out in a previous
181 study [11], including crystal structure, morphology, surface composition and
182 photoelectrochemical characterization.

183

184 2.3. *Preparation of simulated wastewater treatment plant effluent*

185

186 For this study we used simulated wastewater treatment plant effluent (SWWE) as
187 water matrix as previously reported [30] which included: 96 $mg \cdot L^{-1}$ of $NaHCO_3$,
188 60 $mg \cdot L^{-1}$of $CaSO_4.2H_2O$, 60 $mg \cdot L^{-1}$ of $MgSO_4$, 580 $mg \cdot L^{-1}$ of NaCl and 4 $mg \cdot L^{-1}$
189 of KCl; beef extract (1.8 $mg \cdot L^{-1}$), peptone (2.7 $mg \cdot L^{-1}$), humic acid (4.2 $mg \cdot L^{-1}$),
190 tannic acid (4.2 $mg \cdot L^{-1}$), lignosulfonic acid sodium salt (2.4 $mg \cdot L^{-1}$), sodium lauryl
191 sulfate (0.9 $mg \cdot L^{-1}$), gum arabic from acacia tree (4.7 $mg \cdot L^{-1}$), $(NH_4)_2SO_4$ (23.6
192 $mg \cdot L^{-1}$) and K_2HPO_4 (7.0 $mg \cdot L^{-1}$). The SWWE had a pH, conductivity and
193 concentration of dissolved organic carbon close to 8, 1.4 $mS \cdot cm^{-1}$ and 8.1 $mg \cdot L^{-1}$
194 respectively.

195

196 2.4. *EAP degradation of a mixture of CECs in a one-compartment cell*

197

198 The EAP degradation of a mixture of four CECs, trimethoprim (TMP), diclofenac
199 (DFC), sulfamethoxazole (SMX) and carbamazepine (CBZ), in SWWE was
200 evaluated. Experiments were performed in a one-compartment EAP cell, Figure
201 1. A scheme and pictures of the experimental set up that was used to assess the
202 performance on the degradation of a mixture of CECs can be found in the
203 supplementary information (Figure S1). The irradiation source was a 1000 W Xe
204 lamp with AM 1.5 filter. The EAP cell was a 30 mL 3D-printed reactor made of
205 acrylonitrile butadiene styrene (ABS). A power supply (PLH 120 DC power
206 supply, RS) to apply a cell potential, a reservoir tank and a pump (Cole-Parmer,
207 model 7521-10) to continuously flow the solution through the system. The
208 photoanode was irradiated back-face through a 6.1-cm-diameter window and the
209 flow was 0.15 $L \cdot min^{-1}$. The electrical contact was provided by direct contact
210 between the edges of the electrodes and a copper frame. To reduce heating of
211 the cell, an infrared filter (with ultrapure water) was located between the Xe lamp
212 and the electrochemical cell. When the activity of the photoanode was tested
213 under visible only irradiation, a UV cut-off filter was used, which only transmitted
214 radiation with a wavelength higher than 415 nm. The spectral intensity of the
215 incident radiation was determined by using a spectral radiometer (Ocean Optics
216 B.V, Netherlands) (Figure S3). The WO_3 photoanodes (8.4 cm x 8.4 cm or 2 cm
217 x 1.5 cm) were used as working electrodes and a Pt plate (umicore Electroplating,
218 Platinode®) or carbon paper (Ion Power, SIGRACET® Gas Diffusion Media,
219 Type GDL 38 BC) as counter electrode. The temperature of the solution was ~25
220 ºC. When air was flown behind the cathode, the part where the cathode was
221 placed featured a closed chamber with a port to purge air (Figure 1 A and B).
222 When air was not purged, the part where the cathode was place had a 6.1-cm-
223 diameter window to allow air diffusion through the carbon GDE (Figure 1 C and
224 D).

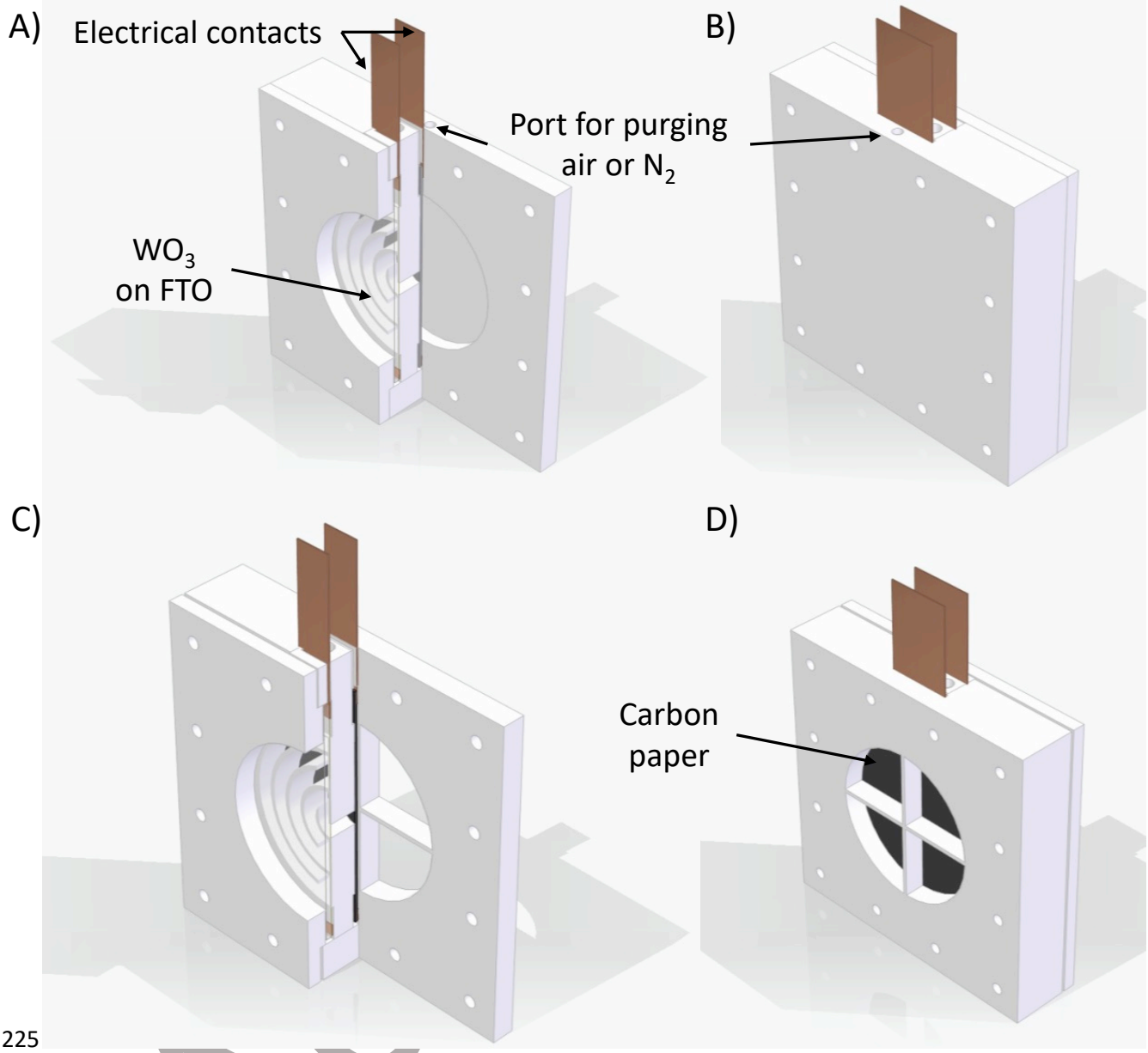

Figure 1. One compartment EAP cell used for the degradation of CECs in simulated wastewater when air or N_2 was purged (A and B) and when no air was purged (C and D).

A stock solution with all the CECs (2.5 $g \cdot L^{-1}$ of each CEC) in methanol was prepared, following the procedure described in other studies [18,31]. The stock solutions with high concentrations of CECs to minimize the amount of methanol added to the water matrix. In a usual experiment, a certain volume of the stock solution was spiked in 200 mL of the SWWE to obtain the desired initial concentration of each CEC (100 $\mu g \cdot L^{-1}$), and the mixture was transferred to the tank where it was continuously stirred. The methanol from the stock contributed an additional TOC concentration of 11.5 mg L^{-1}. Thus, when simulated wastewater was used the initial TOC concentration was near 19.5 mg L^{-1}. The

solution was pumped through the system for 30 minutes in the dark to attain adsorption equilibrium and the Xe lamp was switched on so that the emission would become stable. Then, a few mLs of the solution were taken out, the cell potential was applied and the reactor was irradiated. When air was bubbled into the solution or in the chamber behind the cathode an air blower was employed. Samples were withdrawn every 15 min for the first hour and subsequently every 30 min. Samples were filtered using PTFE hydrophilic syringe filters (Ossila) with 0.45 μm pore size prior to analysis. The optimum applied cell potential was determined by sweeping the potential from 0 V to +2.0 V, with a step of 0.1 V, in dark and under irradiation and measuring the current response with a multimeter. The optimum potential was chosen as the lowest applied potential at which the photocurrent density was maximum.

For scavenger studies, potassium iodide (KI) was used as a hole scavenger, isopropanol as a $HO^{\cdot}$ scavenger, and hydroquinone and p-benzoquinone were used to scavenge $O_2^{\cdot-}$. The initial concentration of each scavenger added was 5 mM. When the experiment required absence of O_2, oxygen free N_2 was purged in the system for 30 min before the experiment began and Na_2SO_3 was added to the solution as an oxygen scavenger [32].

A two-compartment cell previously reported [33] was used to investigate the ROS generated at each electrode (Figure S2). The compartments were magnetically stirred, and a cation membrane was placed to separate them and prevent interference with the working electrode. The EAP cell was operated as a 3-electrode set-up with the WO_3 photoanode, carbon GDE cathode and a saturated calomel electrode (SCE) reference electrode. The anode potential was 0.95 V (SCE), selected to maintain a cell potential of ~1.5 V. The volume added to each compartment was 35 mL. All the experiments were performed using an electrochemical workstation (AUTOLAB PGSTAT 30) and the photoanode was back-face irradiated with a 450 W xenon lamp (Horiba Jobin Yvon FL-1039/40) equipped with an IR water filter and an AM 1.5 filter, as it represents the average annual air mass value at locations within the continental US and Europe [34]. In this case, the incident average UVA (315-400 nm) radiation was around 25 $W \cdot m^{-2}$. In the 415-480 nm range, the irradiance was 61 $W \cdot m^{-2}$ and the spectral distribution very similar to solar spectrum. The irradiance was obtained with a

spectral radiometer (Ocean Optics B.V, Netherlands) and the spectrum is shown in the supplementary information (Figure S4). The irradiance between 200 and 480 nm was 86 $W \cdot m^{-2}$.

The concentration of the CECs was detected and quantified by using an HPLC system (Agilent Technologies Series 1260 Infinity II) equipped with a UV detector and an analytical column Poroshell 120 EC-C18 (4.6x100 mm). The injection volume was 100 μL and the detection wavelengths for TMP, SMX, CBZ and DFC were 267, 273, 273 and 285 nm, respectively. A gradient method was used: from 95/5 (v/v) of formic acid (25 mM)/acetonitrile (ACN) to 20/80 (v/v) of formic acid (25 mM)/ACN after 13 min, from 20/80 (v/v) to 0/100 (v/v) until 14 minutes and a posttime of 3 min, with a flow rate of 1 $mL \cdot min^{-1}$. The temperature was set to 30 ºC. The limit of quantification (LOQ) was calculated for the different parent compounds. The LOQ values were 0.8, 1.5, 0.6 and 0.8 μg L^{-1} for TMP, SMX, CBZ and DCF.

Different probes and methodologies were followed to detect and quantify the potential ROS that can be formed in the EAP process. The concentration was chosen based on previous experience obtained from several studies performed in our research group and from other reported studies [18,33,35–37].

Hydroxyl radicals ($HO^{\cdot}$) were detected by using coumarin as a probe that reacts with $HO^{\cdot}$ to generate different by-products, among them umbelliferone [38]. The initial concentration of coumarin dissolved in SWWE was 0.4 mM. The concentration of umbelliferon was quantified by using an HPLC (described above). The injection volume was 100 μL and the detection wavelength were 250, 270 and 325 nm, respectively. A gradient method was used: 90/10 (v/v) of formic acid (25 mM)/methanol for the first 6.6 minutes, from 90/10 (v/v) of formic acid (25 mM)/methanol to 66.5/33.5 (v/v) of formic acid (25 mM)/methanol in the range 6.6-13.20 min, and from 66.5/33.5 (v/v) to 50.5/49.5 (v/v) up to 26.5 minutes and a post time of 3 min. The flow rate was 0.5 $mL \cdot min^{-1}$ and the temperature 30 ºC.

Hydrogen peroxide (H_2O_2) was quantified by a spectrophotometric method in which 1.5 mL of the sample was mixed with 1.5 mL of a 280 mM $TiOSO_4$ solution [36]. The absorbance of the yellow complex was measured using a JENWAY 6305 spectrophotometer at 410 nm.

Superoxide radical ($O_2^{\cdot-}$) generation was assessed by monitoring the degradation of hydroquinone in the presence of a KI as a h^+ scavenger (5 mM) to avoid its oxidation by holes or $HO^{\cdot}$ [39]. Because of the higher selectivity of hydroquinone towards $O_2^{\cdot-}$ [40], it reacts with superoxide radicals to produce p-benzoquinone. The concentration of hydroquinone was quantified using an HPLC (described in section 2.4). A simple isocratic method was adopted: 0.5 $mL \cdot min^{-1}$, 80/20% v/v formic acid (25 mM)/methanol. The injection volume was 5 µL and the temperature 30 ºC. The detection wavelengths were 290 and 250 nm.

Free chlorine (FC) was also measured using a photometer system (Chlorine+ eXact® EZ, Industrial Test systems, Inc.) and eXact® Strip Micro Free Chlorine (DPD-1).

3. Results and discussion

3.1. *Comparison of CECs degradation using Pt or GDE as a cathode*

The performance of the EAP cell using a carbon GDE as a cathode was compared to that using Pt for the degradation of a mixture of 4 CECs in simulated wastewater effluent (SWWE). The use of the GDE removes the need to sparge the electrolyte with air or oxygen [33]. The optimal cell potentials were +1.3 for the Pt CE and +1.5 V for the carbon GCE CE (Figure S5).

The degradation profiles for the mixture of CECs obtained when using the Pt cathode are shown in Figure 2 along with the controls i.e., fixed potential in the dark (EC) and the photocatalytic reaction (under irradiation and open circuit).

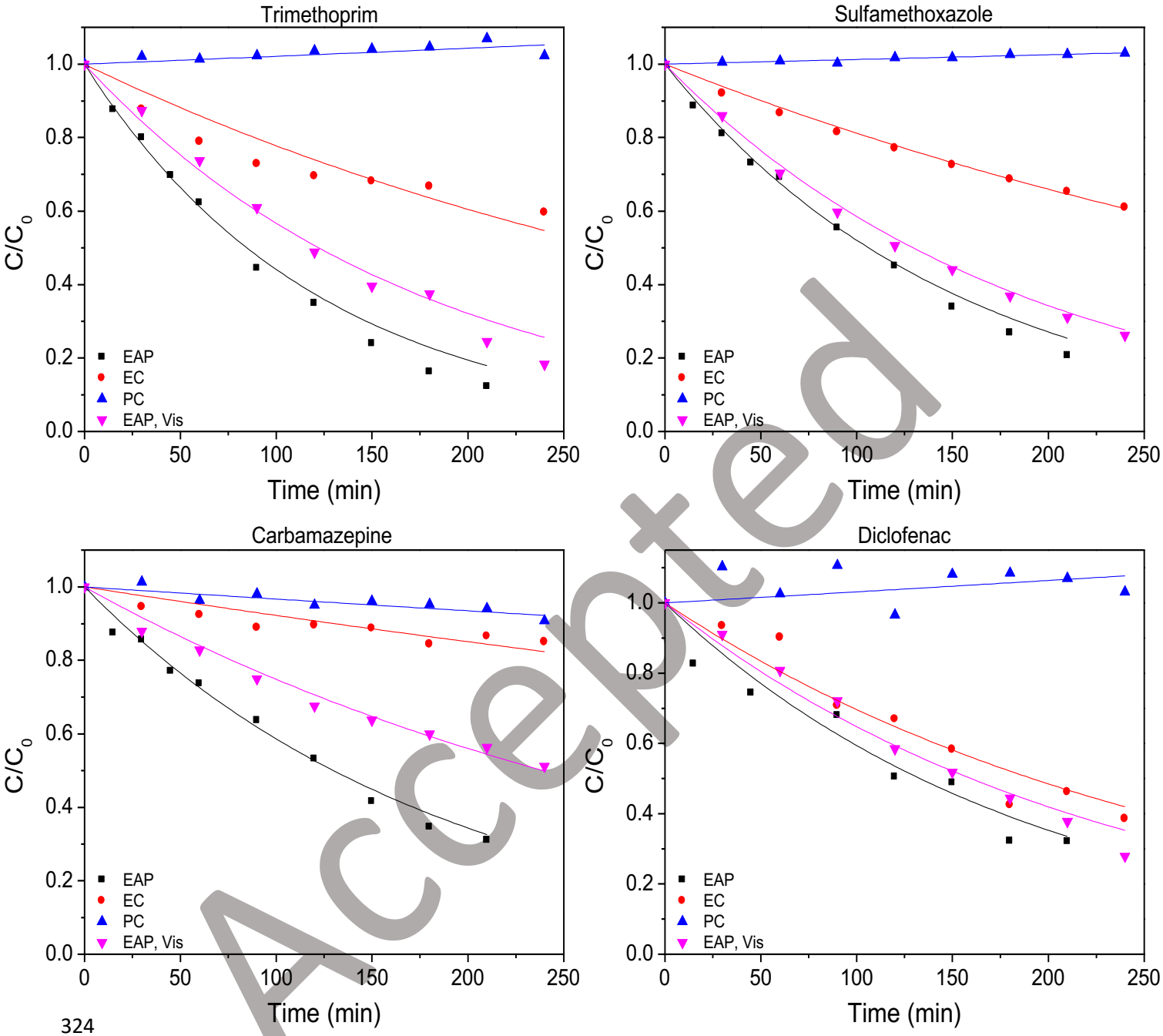

Figure 2. Concentration of CECs simulated wastewater effluent vs time with electrochemically assisted photocatalysis (EAP) experiments in under the following conditions: WO_3 was used as a photoanode and Pt as a cathode, $[CECs]_0$=100 μg·L^{-1}, V_T=200 mL, $I_{0,\ EAP}$ (200-480 nm)=86 W·m^{-2}, $I_{0,\ EAP\ Vis}$ (415-480 nm)=61 W·m^{-2}, cell potential=1.3 V and irradiated area=29 cm^2. Legend: ■ Electrochemically Assisted Photocatalysis (EAP), ● Electrocatalysis (EC), ▲ Photocatalysis (PC), ▼ Electrochemically Assisted Photocatalysis with only visible light (EAP,Vis).

All the CECs, except CBZ, showed significant degradation with electrocatalysis in the dark (EC). The kinetic constants were estimated assuming pseudo-first order reaction rate (Table 1). When the electric potential was applied under

irradiation (EAP) a significant increase in CEC degradation was observed, with three times the rate observed for TMP or SMX, as compared to EC. CBZ is reported as one of the most persistent and difficult to degrade CECs [17,41,42]. The rate constant for CBZ degradation was 5.34 x10^{-3} min^{-1} for EAP as compared to only 0.81 x10^{-3} min^{-1} for EC. More importantly, the WO_3 photoanode showed marked activity under visible only irradiation. Even though the irradiation for the EAP experiments using the UV cut-off filter was almost two thirds of the value under the whole spectrum, 61 and 86 $W \cdot m^{-2}$, rate constants $5.67 \cdot 10^{-3}$, $5.35 \cdot 10^{-3}$, $2.9 \cdot 10^{-3}$ and $4.35 \cdot 10^{-3}$ min^{-1} were estimated for TMP, SMX, CBZ and DFC, proving the viability of using WO_3 as a photoanode under solar radiation to drive the EAP process. This is a significant advantage of using WO_3, where the band gap (2.6 eV) is smaller than that of TiO_2 (3.2 eV) [10]. Furthermore, it can be concluded that in the photocatalytic experiment (at open circuit potential) the CECs underwent no degradation. This behaviour is different to the results reported previously using TiO_2. Salmeron et al. [18] observed similar removal efficiences in the photocatalytic and EAP degradation of a mixture of organic micro-polluants using TiO_2 nanotubes as photoanode. These results were ascribed to the organic matter present in the water matrix, which scavenge oxidizing species. Similarly, Tang et al. [20] observed conversions of tetracycline close to 88% and 100% after 120 min of the photocatalytic and EPA reactions using g-C_3N_4 nanosheets implanted into TiO_2 nanotubes. Pablos et al. [43] also observed no differences in the oxidation of methanol with and without applied potential. They stated that applying an electric bias will lead to an improvement in the degradation of chemical compounds when charge interactions between a photoanode and the target are highly influential, hence reducing mass transfer limitations. However, when WO_3 was used as photocatalyst no degradation was expected as the conduction band potential (~+0.7 V vs SHE) [11,19] is more positive than the potential required to carry out possible reduction reaction, such as the reduction of oxygen to produce superoxide radicals ($e^-_{BC} + O_2 \rightarrow O_2^{\cdot -}$, -0.33 V SHE, pH 0) or the reduction of protons to form hydrogen ($2e^-_{BC} + 2H^+ \rightarrow H_2$, 0.0 V SHE, pH 0) (Figure 3) [33]. Therefore, for WO_3 to be used as a photocatalyst an electron acceptor would have to be added.

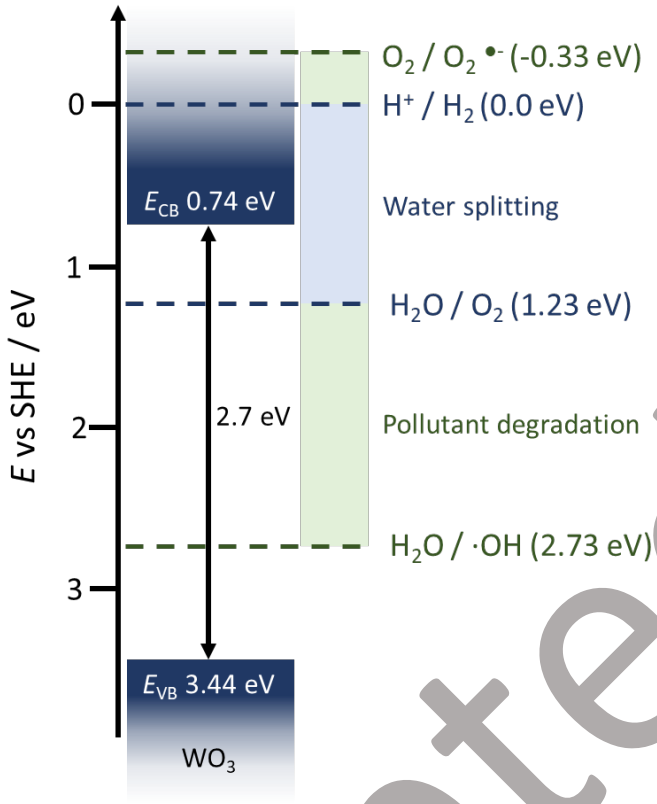

367

368 **Figure 3**. Band diagram of WO_3 at pH 0 with the conduction band edge (E_{CB}) and
369 valence band edge (E_{VB}) positions shown, with the key reactions for pollutant
370 degradation and water splitting.

371 **Table 1**. Pseudo-first order reaction rate constants and 95% upper and lower
372 confidence intervals (UCI / LCI) estimated for the degradation of each CEC in SWWE
373 using WO_3 as photoanode and a Pt sheet or carbon paper (CP) as a cathode.

		WO_3-Pt			WO_3-CP			
		k (min^{-1})x10^3						
		EAP	**EC**	**EAP, Vis**	**EAP**	**EC**	**EAP, Vis**	**No air flow**
TMP		8.18	2.51	5.67	6.28	1.6	4.22	8.72
SMX		6.52	2.08	5.35	5.99	1.4	4.33	9.24
CBZ		5.34	0.81	2.9	3.72	0.67	3.03	5.16
DFC		5.21	3.62	4.34	4.07	2.5	2.97	7.57
		LCI / UCIx10^3						
		EAP	**EC**	**EAP, Vis**	**EAP**	**EC**	**EAP, Vis**	**No air flow**
TMP	LCI	7.85	2.1	5.47	6.13	1.41	4.17	8.54
	UCI	9.05	3.1	6.52	7	1.83	4.51	9.49
SMX	LCI	6.62	2.03	5.27	5.95	1.39	4.23	9.02
	UCI	7.28	2.2	5.5	6.78	1.45	4.53	10.12
CBZ	LCI	5.22	0.66	2.74	3.47	0.53	2.85	4.78
	UCI	5.89	0.98	3.13	4.03	0.83	3.34	5.88
DFC	LCI	4.66	3.21	4.05	3.61	2.53	2.7	7.22

UCI	6.33	4.3	4.89	4.84	2.92	3.58	9.38

When carbon paper was used as a cathode with air flowing behind the cathode, similar trends were observed for the degradation of each CEC (Figure S6) compared to the obtained with Pt, i.e., neither adsorption nor degradation was observed with photocatalysis (open circuit) and significant rates of degradation were attained under visible light. The degradation rates decreased slightly, but the kinetic constants were always 75% of those estimated with Pt as a cathode (shown in the supplementary information, Table 1). No significant reduction in TOC was observed, as the contribution of CECs to the TOC was far smaller than the TOC from the organic matter present in the SWWTE. Owing to the lower cost and similar performance of the carbon GDE as compared to the Pt, it was selected as cathode for all other experiments.

3.2. *Effect of air flow in the WO_3-carbon paper GDE system*

In order to evaluate the effect of O_2 in the EAP process when carbon GDE was used as a cathode, different experiments were performed (Figure S7) pumping air, either into the storage tank or into the chamber at the back of the cathode, and without pumping air (the GDE was open to air, see Figure 1), e.g., letting atmospheric air diffuse through the carbon paper.

According to the degradation profiles, pumping air did not lead to faster degradation kinetics for all the CECs. Lower current densities have also been detected when higher air flows were used since the formation of bubbles can increase ohmic resistance [33]. Moreover, even though ROS generated via O_2 reduction might not be important, electrons can still play a part in the process via H_2O_2 electro-activation through an electron transfer reaction at the cathode or through direct reduction of the pollutants [44]. It is important to note that when air was not pumped, the reaction rates were even faster than the attained when Pt was utilized as a cathode (see kinetic constants in Table 1), achieving values of $8.72 \cdot 10^{-3}$, $9.24 \cdot 10^{-3}$, $5.16 \cdot 10^{-3}$ and $7.57 \cdot 10^{-3}$ min^{-1} for TMP, SMX, CBZ and DFC.

From here on now, all the experiments were carried out without pumping air unless stated otherwise.

3.3. *Effect of water matrix in the WO_3-CP system*

To examine the influence of the water matrix on the degradation of the mixture of CECs in SWWE, experiments were undertaken using distilled water where Na_2SO_4 was added to obtain the same electrolyte conductivity as the SWWE (1.4 $mS \cdot cm^{-1}$). The comparison of the degradation results obtained in distilled water with sodium sulfate for the EAP and the control experiments in the dark (EC) and under radiation at open circuit potential (PC) can be seen in the supplementary information (Figure S8). Figure 4 shows a small effect of the water matrix for the degradation of TMP and SMX, attaining conversions of each CEC near 85% in both water matrices. Faster degradation rates were observed for CBZ and especially DFC. A decrease of the degradation performance for all the CECs would be expected in the simulated wastewater as several studies have reported a drop in the process efficiency due to the competition for ROS with the background organic matter and some inorganic ions [42].

Similar results for some of the CECs studied here can be found in the literature. It has been reported that the degradation of SMX was not affected by the presence of Cl^- or SO_4^{2-} in water [45]. Higher degradation of SMX was also detected at acidic pH due to a greater adsorption on TiO_2 [46], as the anionic form of SMX (pKa_2=5.6) will prevail at pH similar to those of the SWWE (pH=8) whereas the neutral form and the anionic form should predominate the pH of the distilled water (pH=6.1). However, since the surface of the photoanode is always positively charged under applied positive bias the difference cannot be ascribed to the electrostatic interactions. In fact, Cai et al. observed similar effects of the pH and concluded that the faster degradation at lower pH was due to a stronger radiation absorption and higher photochemical reactivity of SMX in its neutral form, that leads to shorter half-lives and higher decomposition efficiency [47]. As for TMP (pKa=6.7), they did not note any effect of the pH as described here [47]. Other studies have reported significantly lower degradation rates of DFC at lower

pH. Since in the pH range from 6.1 to 8 it is always negatively charged (pKa=4 [48]), the electrostatic interactions between the photoanode and DFC can favour its degradation.

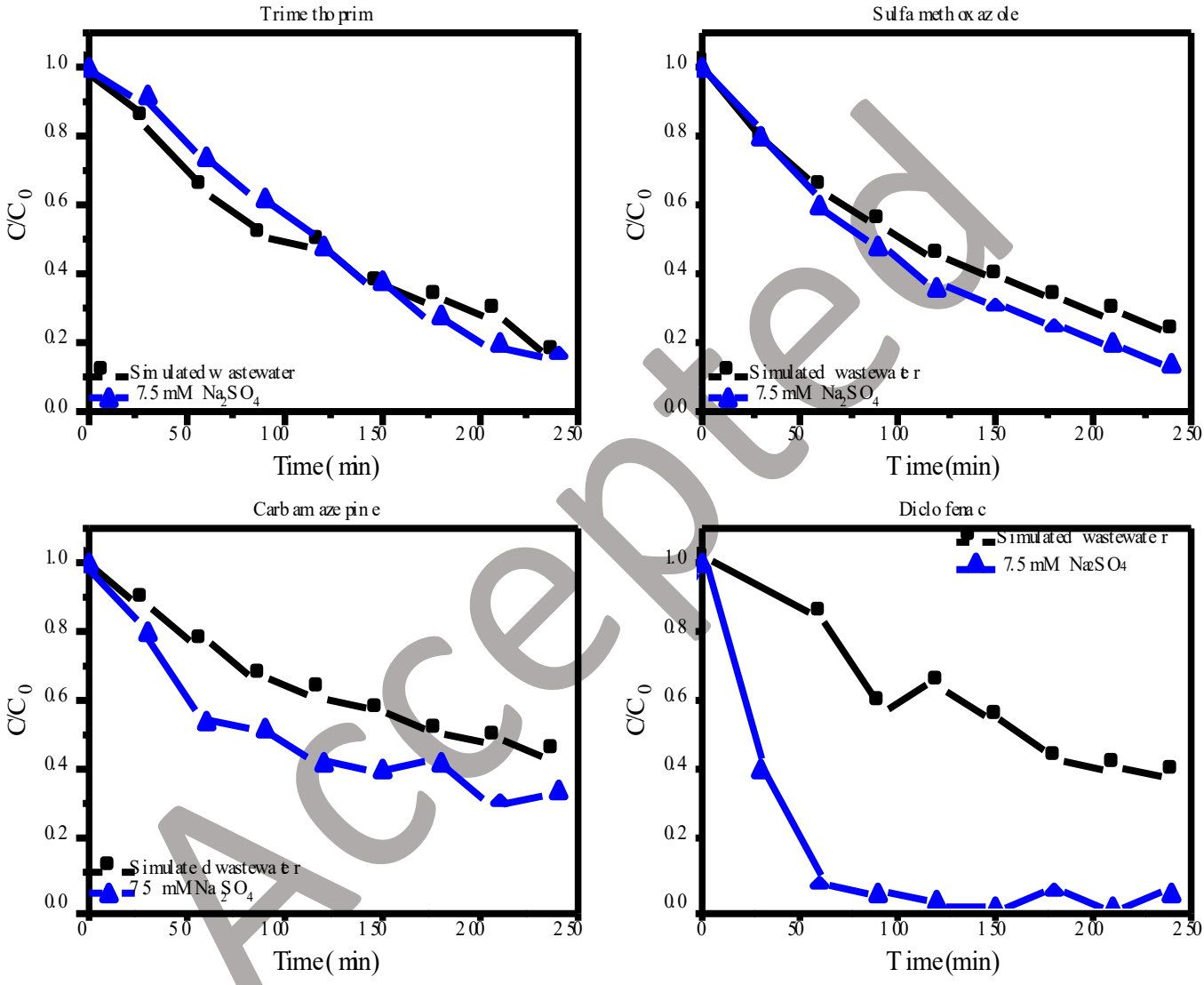

Figure 4. CECs degradation vs time with EAP using simulated wastewater effluent or 7.5 mM Na_2SO_4 solution (in distilled water) as a water matrix. In all the experiments WO_3 was used as a photoanode and carbon paper as a cathode, $[CECs]_0$=100 μg·L^{-1}, V_T=200 mL, solar simulated light, I_0 (200-480 nm)=86 W·m^{-2}, no air was purged in the system, cell potential=1.5 V and irradiated area=29 cm^2.

3.4. *Effect of scavengers and detection of ROS*

In order to elucidate the degradation mechanism and the relevance of the different ROS that can be produced in the EAP process, the degradation reactions were performed in the presence of different scavengers. Potassium iodide (KI), isopropanol, hydroquinone and p-benzoquinone were used to scavenge h^+, $HO^{\cdot}$ and $O_2^{\cdot-}$ respectively [19,45,49–51]. The initial concentration of each scavenger was 5 mM. The results, along the degradation profiles in the absence of scavengers, are depicted in Figure 5. To elucidate to which extent the pollutants are degraded at the anode and at the cathode, a two-compartment cell was used. The cell featured a membrane that separated both compartments to prevent interference and allow the study of the anodic and cathodic reactions and the detection of the main ROS. Figure 6 shows the concentration profiles of each CEC in the anode and cathode compartments.

462

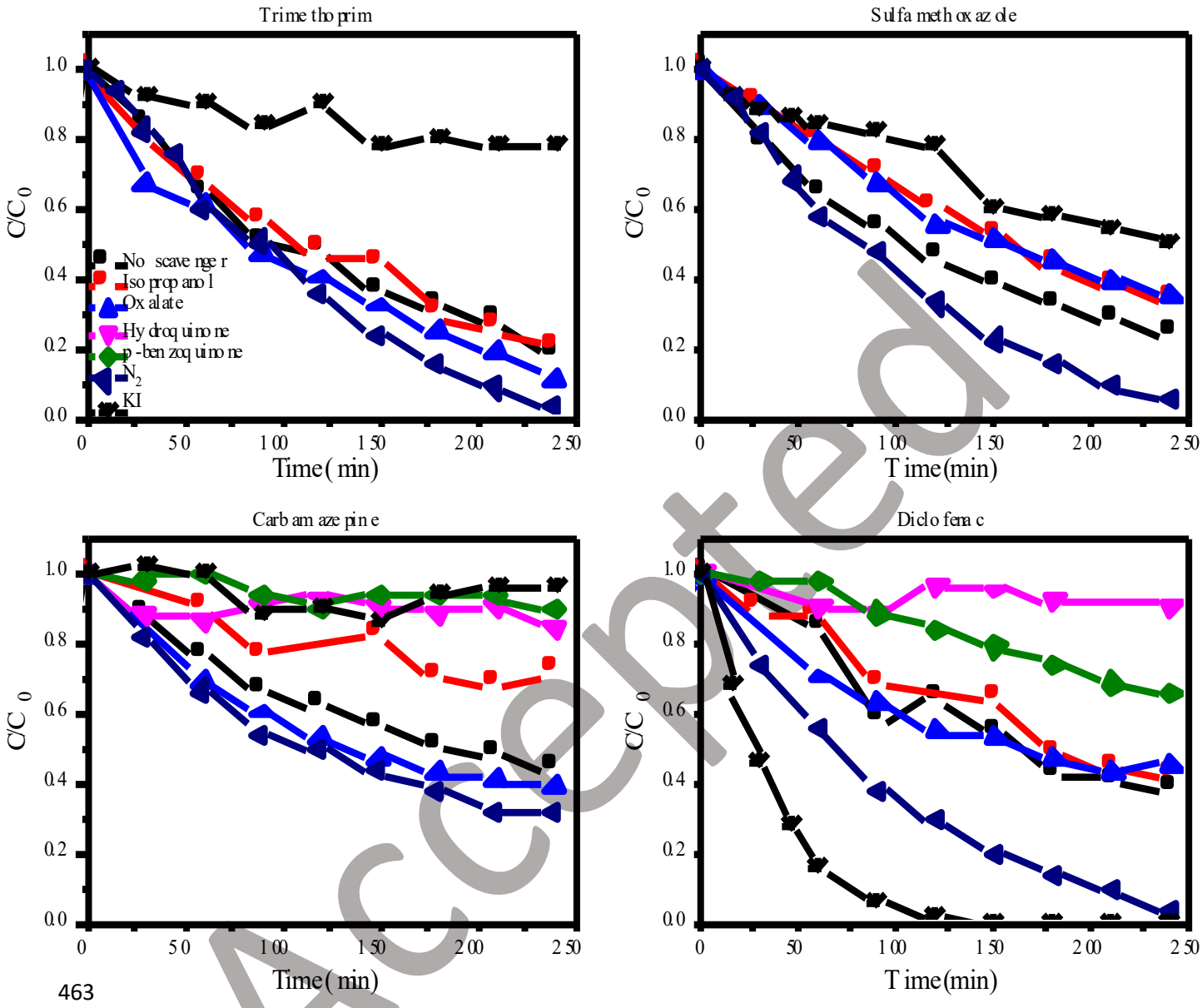

463

464 **Figure 5.** Comparison of CECs degradation over the EAP degradation experiments in
465 the presence of different scavengers (using simulated wastewater effluent as water
466 matrix). In all the experiments WO_3 was used as a photoanode and carbon paper as a
467 cathode, $[CECs]_0$=100 μg·L^{-1}, V_T=200 mL, solar simulated light, I_0 (200-480 nm)=86
468 W·m^{-2}, applied cell potential=1.5 V and irradiated area=29 cm^2. The initial
469 concentration of each scavenger was 5 mM. Legend: ■ no scavenger, ● isopropanol,
470 ▲ oxalate, ▼ Hydroquinone, ♦ p-benzoquinone, ◄ N_2, X KI.

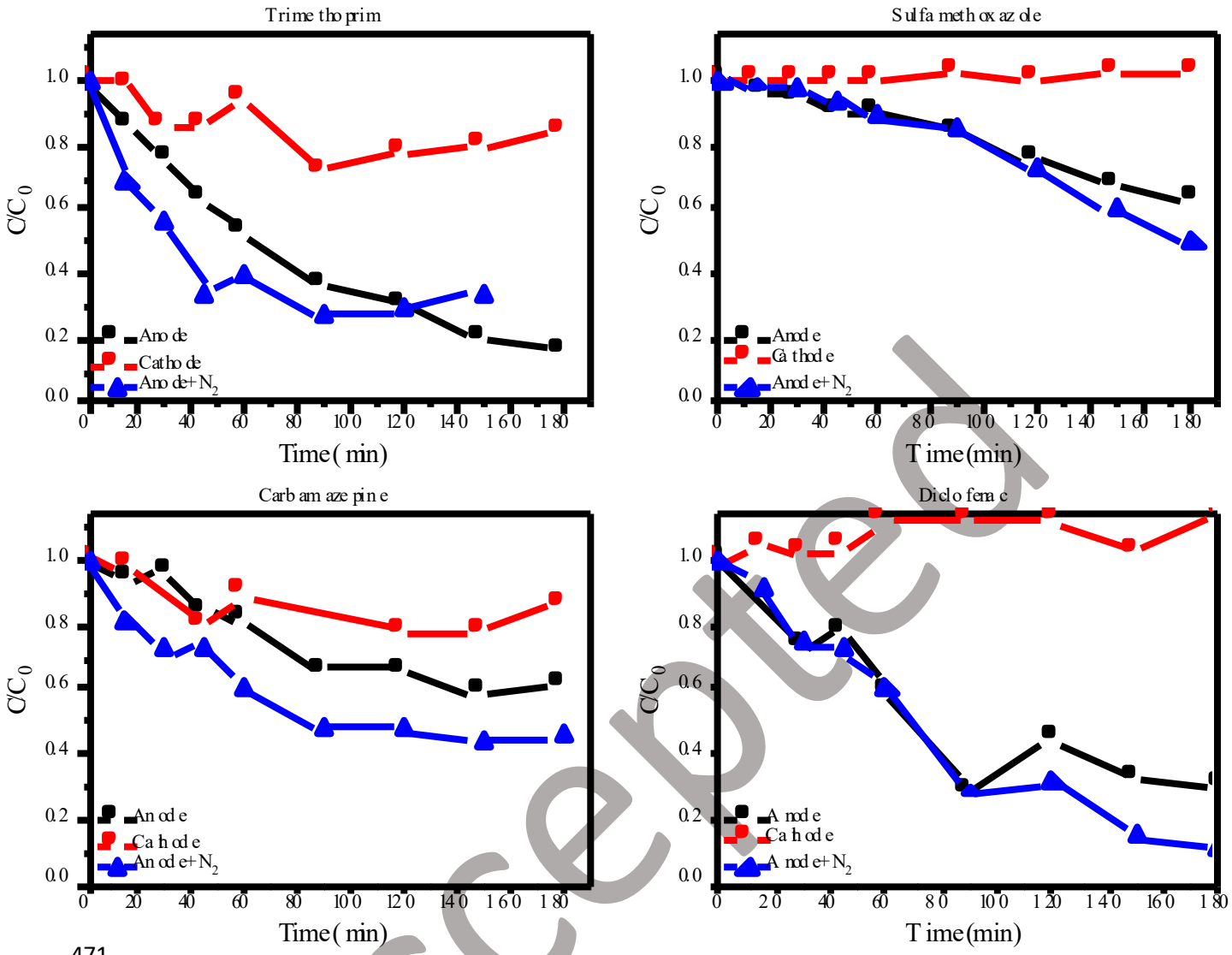

471

472 **Figure 6**. Comparison of CECs degradation over the EAP degradation experiments in
473 the anode and cathode compartment. In all the experiments WO_3 was used as a
474 photoanode and carbon paper as a cathode, $[CECs]_0$=100 μg·L^{-1}, $V_{compartment}$=35 mL,
475 solar simulated light, I_0 (200-480 nm)=19 W·m^{-2}, cell potential=1.5 V and irradiated
476 area=2 cm^2.

477

478 When KI was used to scavenge h^+ there was a considerable decrease in the
479 reaction rate for most of the CECs studied, indicating that h^+ plays a vital role in
480 the EAP process. It is worth mentioning that diclofenac degradation was
481 significantly increased upon the addition of KI. I^- could be easily oxidized by holes
482 into free iodine (FI) which can cause the iodination of diclofenac and formation of
483 by-products since the kinetic constant for the reaction between FI and DFC is
484 large (2000–3000 M^{-1} s^{-1}) [52]. The addition of isopropanol as $HO^{\cdot}$ scavenger
485 did not reduce the degradation rate of the DFC and TMP and the rate of

degradation of SMX and CBZ was slightly reduced. In order to know the performance of the process to produce $HO^{\cdot}$ radicals, coumarin was used as a probe since it reacts with $HO^{\cdot}$ radicals with high selectivity to generate 7-hydroxycourmarin [38]. The concentration of coumarin and 7-hydrodxycoumarin over the reaction time can be seen in Figure S9. The concentration of 7-hydroxycoumarin increases linearly and remains constant after 90 minutes of reaction time while the concentration of coumarin continues decreasing until the end of the reaction. In other words, after 4 hours only 76.4 nmol were formed. The photonic efficiency (η_λ) to produce 7-hydroxycoumarin and the faradaic efficiency (η_e) for the $HO^{\cdot}$ generation was calculated in the supplementary information. The small amount of $HO^{\cdot}$ radical detected and the low efficiencies would suggest a small contribution to the degradation of the studied CECs, especially taking into account the scavenging effect of the organic matter and some ions present in the SWWE. Regarding the degradation results obtained in the two-compartment cell, it could be noted that much higher conversions were obtained for all the CECs in the photoanode compartment and conversions lower than 10% were obtained in the cathode compartment. Experiments were performed to evaluate the generation rate of $HO^{\cdot}$ in both compartments. However, no significant $HO^{\cdot}$ was detected in the cathode compartment and only a small signal, below the quantification limit, was observed in the anode compartment (data not shown). The reason why in this cell we were not able to detect $HO^{\cdot}$ whereas it could be monitored in the one-compartment cell is ascribed to the difference in radiation intensities (I_0 (200-480 nm)=86 $W \cdot m^{-2}$ and I_0 (200-480 nm)=19 $W \cdot m^{-2}$ for the one- and two-compartment cells) and to higher volume to surface ratio of the two-compartment cell. It also explains why for most of the CECs studied, the degradation kinetics were not affected by the presence of the $HO^{\cdot}$ scavenger.

Due to the presence of Cl^- in the water matrix it can be oxidized by holes or $HO^{\cdot}$ radicals to generate various chlorinated reactive radicals, such as chlorine (Cl_2) and hypochloric acid (HOCl), and free chlorine (reactions 1-6) [53–55].

$$Cl^- + h^+ \rightarrow Cl^{\cdot} \qquad E^0(Cl^{\cdot}/Cl^-) = 2.62 \text{ V vs SHE} \quad 1$$

$$Cl^- + HO^{\cdot} \rightarrow ClOH^{\cdot -} \quad 2$$

$$ClOH^{\cdot -} + H^+ \rightarrow Cl^{\cdot} + H_2O \quad (3)$$

$$Cl^{\cdot} + Cl^- \rightarrow Cl_2^{\cdot -} + H_2O \quad (4)$$

$$Cl_2^{\cdot -} + Cl_2^{\cdot -} \rightarrow Cl_2 + 2Cl^- \qquad E^0(Cl_2/Cl_2^{\cdot -}) = 1.36\ \text{V vs SHE} \quad (5)$$

$$Cl_{2\,(aq)} + H_2O \rightarrow HOCl + H^+ + Cl^- \qquad E^0(HOCl/Cl^-) = 1.49\ \text{V vs SHE} \quad (6)$$

The free chlorine concentration was measured over the experiment, but after 4 hours only 0.28 mg·L^{-1} were formed, which is below the recommended free chlorine level for residual disinfection of water [56]. Thus, it can be confirmed that the degradation of the CECs was not likely to be caused by reactive Cl species.

Even though sulfate radicals can be generated from the SO_4^{2-} present in the simulated wastewater effluent and oxidize organic compounds, it has been reported that they are more easily generated at acidic pH to avoid the hydrolysis of $SO_4^{\cdot -}$ into $HO^{\cdot}$ [53]. Also it has been reported that the availability of $SO_4^{\cdot -}$ is considerably decreased in the presence of Cl^- because chlorides scavenge $SO_4^{\cdot -}$ [53]. This effect was also observed by Gao et al. [54] who reported a marked inhibition on the triclosan conversion at concentration of Cl^- below 10 mM, detecting a small amount of free chlorine.

As H_2O_2 can also play a key role in the EAP process and lead to the generation of more $HO^{\cdot}$, the formation of H_2O_2 in the one-compartment cell was assessed (Figure 7) without purging air in the system.

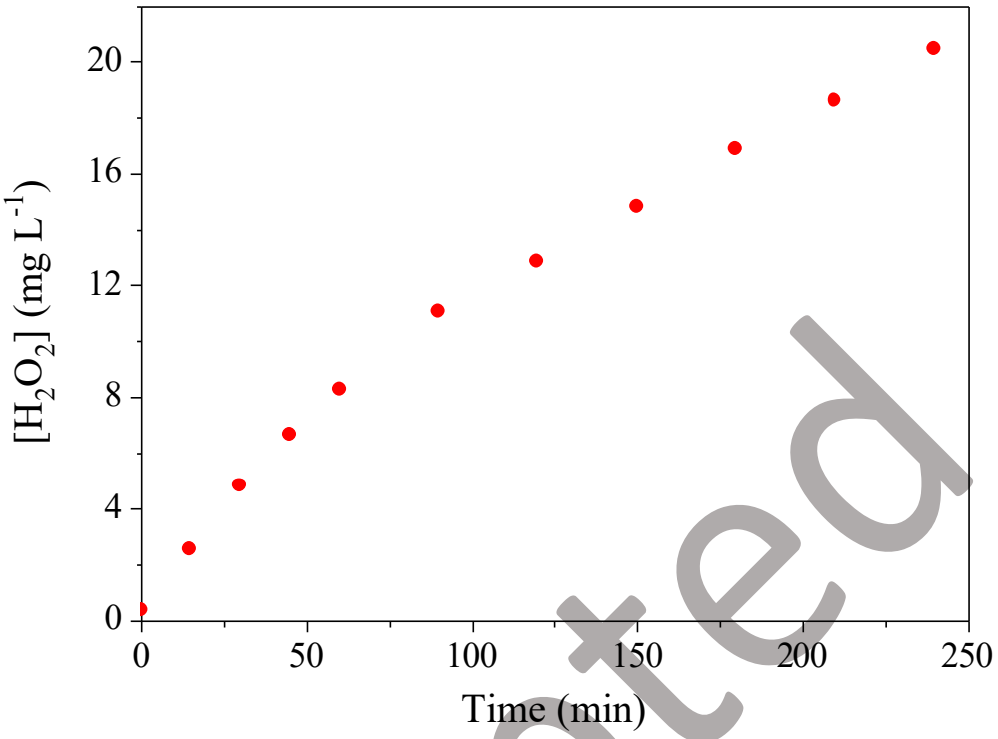

Figure 7. Comparison of H_2O_2 production over the EAP degradation experiments in the one-compartment cell (using simulated wastewater effluent as water matrix) without pumping air. In the experiment WO_3 was used as a photoanode and carbon paper as a cathode, $[CECs]_0$=100 μg·L^{-1}, V_T=200 mL, solar simulated light, I_0 (200-480 nm)=86 W·m^{-2}, applied potential=1.5 V and irradiated area=29 cm^2.

Significant concentrations of H_2O_2 were produced at the cathode and the Faradaic efficiency for the electrogeneration of H_2O_2 was calculated according to the following equation:

$$\eta_e = \frac{molecules\ \ formed}{Number\ of\ electrons} = \frac{C_{H_2O_2} \cdot V_R \cdot n \cdot F}{\int_0^t I dt} \qquad Eq.1$$

Where $C_{H_2O_2}$ is the concentration of H_2O_2 generated, V_R is the total reaction volume, n is the number of electrons transferred for H_2O_2 (2), F the Faraday constant (96,486 C/mol), I is the photocurrent and t the reaction time. A Faradaic efficiency close to 54% was obtained. This reasonable Faradaic efficiency for the production of H_2O_2 could be very advantageous for the inactivation of bacteria

since H_2O_2 has been reported to be a key ROS for disinfection. Few EAP studies monitored the H_2O_2 production, any that did have reported lower Faradaic efficiencies. Salmeron et al. [18] was not able to detect any H_2O_2 during the EAP removal of CECs in a EAP cell in which TiO_2 nanotubes were used as photoanode and carbon felt as cathode. Daghrir et al. [57] compared the production of H_2O_2 using different cathodes (applying 0.39 A in a EAP with Ti/TiO_2 as photoanode) and found out that the highest generation was attained with vitreous carbon, 0.2 mmol/L (Faradaic efficiency close to 3.3%). Therefore, the studied EAP system seems promising for the simultaneous degradation of CECs and inactivation of microorganisms. H_2O_2 can also be generated on the photoanode through the two-hole oxidation of H_2O to form H_2O_2 (reactions 7,8) [40].

$$2h^+ + 2H_2O \rightarrow H_2O_2 + 2H^+ \quad (7)$$

$$2HO^{\cdot} \rightarrow H_2O_2 \quad (8)$$

The H_2O_2 concentration formed at the anode and at cathode of the two-compartment cell was measured. H_2O_2 was only produced at the cathode (Figure 8) reaching a concentration just over 11 $mg \cdot L^{-1}$ after 150 min (the measured current was around 430 μA). The Faradaic efficiency for H_2O_2 production was 55.8%, similar to that obtained in the one-compartment cell, verifying that H_2O_2 is only generated at the cathode. Since no $HO^{\cdot}$ was detected in the cathode compartment it can be concluded that $HO^{\cdot}$ was not generated by the one electron reduction of H_2O_2 (reaction 14). This agrees with the results reported by other authors, which stated that carbonaceous cathodes and gas-diffusion electrodes have low catalytic activity towards H_2O_2 decomposition [58,59]. It is noteworthy that despite the production of H_2O_2 at the cathode no relevant degradation of the CECs was attained. This is related to the fact that H_2O_2 is only a moderate oxidant whose standard apparent redox potential is lower at basic pH than at acid pH (1.77 V vs SHE and 0.88 V vs SHE at acid and basic pH). Hence, it is unable to attack phenol and it is only able to degrade some organics such as aldehydes or formic acid [44].

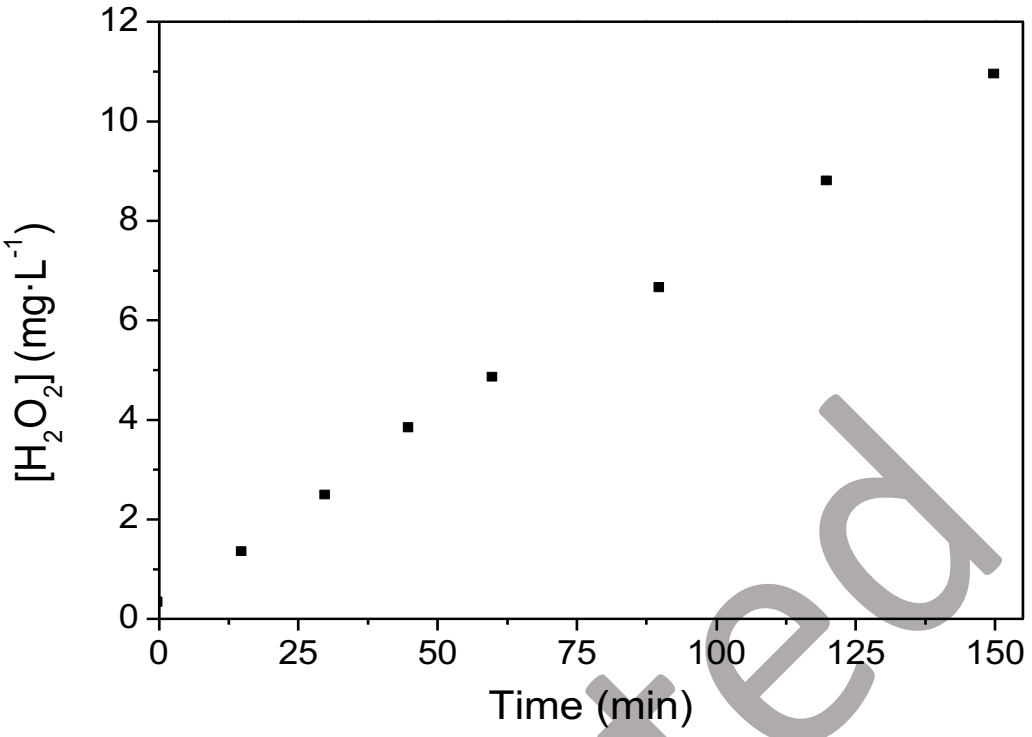

585

586 **Figure 8**. H_2O_2 concentration vs time in the cathode compartment for EAP in the two
587 compartment cell. WO_3 was used as a photoanode and carbon GDE as a cathode,
588 $[CECs]_0$=100 μg·L^{-1}, $V_{compartment}$=35 mL, solar simulated light, I_0 (200-480 nm)=19 W·m^{-2},
589 cell potential=1.5 V and irradiated area=2 cm^2.

590

591 Para-benzoquinone and hydroquinone have been used to evaluate the role of $O_2^{\cdot-}$
592 [37,39,40]. Looking at the concentration profiles of CBZ and DFC (Figure 5) no
593 degradation was observed in the presence of neither of the $O_2^{\cdot-}$ scavengers, which
594 seemed to indicate that $O_2^{\cdot-}$ plays an important part in the process. However, as
595 discussed in the supplementary information the use of quinones to detect
596 superoxide radicals is subject to interferences and results have to be interpreted
597 carefully. In fact, when N_2 was purged into the system (to evaluate the role of the
598 different ROS generated via oxygen reduction, reactions 9-14), the degradation
599 of the CECs was not affected, entailing that electrons or ROS generated at the
600 cathode do not play an important part in the degradation mechanism of these
601 CECs.

602 $$e^-_{BC} + O_2 \rightarrow O_2^{\cdot-} \qquad E^0 = -0.33\ \text{V vs SHE} \qquad 9$$

603 $$O_2^{\cdot-} + H^+ \rightarrow HO_2^{\cdot} \qquad E^0 = -0.05\ \text{V vs SHE} \qquad 10$$

$$O_2 + 2H^+ + 2e^- \rightarrow H_2O_2 \qquad E^0 = 0.695\ \text{V vs SHE} \qquad (11)$$

$$H_2O_2 + O_2^{\cdot-} \rightarrow HO^{\cdot} + O_2 + HO^- \qquad (12)$$

$$2O_2^{\cdot-} + 2H_2O \rightarrow 2HO^{\cdot} + O_2 + 2HO^- \qquad (13)$$

$$H_2O_2 + e_{Cb}^- \rightarrow HO^{\cdot} + HO^- \qquad E^0 = 0.31\ \text{V vs SHE} \qquad (14)$$

Concerning the $O_2^{\cdot-}$ production in the two-compartment cell, hydroquinone degradation was monitored to determine whether some electrons can still reduce O_2 at the anode. To prove that the decrease in hydroquinone concentration was driven by the attack of $O_2^{\cdot-}$ several controls (applied potential in the dark, EC; EAP at open circuit potential, PC and EAP process purging N_2, EAP+N_2) were performed. The evolution of hydroquinone concentration at both electrodes is plotted in the supplementary information, Figure S10. The profiles were fitted to a zero-order kinetic and the reactions rates are collected in Table 2.

Table 2. Degradation rates of hydroquinone under different operating conditions.

	(-r) (mg·L^{-1}·min^{-1})			
	EAP	**EAP+N_2**	**PC**	**EC**
Anode	0.40	0.31	0.36	0.38
Cathode	0.41	0.27	0.23	0.22

Hydroquinone degradation was similar for the PC and EC controls in both compartments. With the PC control O_2 reduction would not be expected due to the positive conduction band potential of WO_3 (as explained in section 3.1). Therefore, hydroquinone degradation may be due to thermal oxidation and oxidation by O_2 since the pH>7 [39,60], giving rise to p-benzoquinone. However, even when N_2 was purged in the system the concentration of hydroquinone decreased. This decrease was not caused by oxidation since no p-benzoquinone was detected, as shown in the chromatograms in Figure S11. However, in the chromatograms of the EAP+N_2 new peaks that didn't appear in the EAP, PC and EC experiments were identified (Figure S11), pointing out some interaction among KI and hydroquinone in the absence of O_2. During the EAP experiment in the cathode compartment a higher degradation rate for the HQ (compared to the

controls) was observed, which indicated the production of $O_2^{\cdot-}$. However, it could be noted that the degradation rates of hydroquinone at the anode were similar for all the experiments, which means that hydroquinone was being degraded only by thermal oxidation and oxidation by O_2. Moreover, these results confirmed that hydroquinone and p-benzoquinone must be used as $O_2^{\cdot-}$ scavengers with care because they can react with h^+ inhibiting the CECs mineralization. Furthermore, owing to the negligible concentration of $HO^{\cdot}$ measured at the anode, it can be concluded that CECs were mainly degraded by photogenerated h^+ and $HO^{\cdot}$ may play a role in the degradation of SMX and CBZ, although to a minor extent. This was confirmed by looking at the degradation profiles of the CECs when N_2 was purged in the anode compartment (Figure 6), which did not affect their reaction rates.

3.5. *Calculation of energy consumption: "Electric energy per order"*

Since economics is often the most relevant parameter and advanced oxidation technologies (AOTs) usually consume considerable amount of energy, different figures-of-merit were proposed related to the electric-or solar-energy efficiency [61]. In this study the electric energy per order, E_{EO} ($kWh \cdot m^{-3} \cdot order^{-1}$) was calculated, using equation 2, to evaluate the EAP process. This metric is suitable for electric-energy-driven systems when working with low concentrations. It is the electric energy in kilowatt hours (kWh) required to degrade a contaminant C by one order of magnitude, for example from 10 mg L^{-1} to 1 mg L^{-1}, in a unit volume (e.g., 1 m^3) of contaminated water.

$$E_{EO} = \frac{P \cdot t \cdot 1000}{V \cdot log(C_i/C_f)} \qquad Eq.2$$

where P stands for the rated power (kW) of the treatment system, t being the treatment time (h), V the treated volume (0.2 L) and C_i and C_f the initial and final concentrations of the pollutant after the t treatment time. The treatment time considered for the CECs removal was 4 h. Since in a real application the EAP system would be solar-driven and the irradiation source was only employed to simulate solar conditions, the energy input corresponding to the Xe lamp was not

taken into account. The E_{EO} values were calculated for the EAP degradation of pollutants using simulated wastewater and without purging air. Given that for that experiment the average current response was 4.98 mA, the E_{EO} values were 0.15, 0.16, 0.32, 0.22 kWh·m^{-3}·order^{-1} for TMP, SMX, CBZ and DFC. When the radiation source was taken into account, the electric energy per order increased drastically. The values of E_{EO} are 19.8·10^3, 21.8·10^3, 42.2·10^3 and 29.5·10^3 kWh·m^{-3}·order^{-1} for TMP, SMX, CBZ and DFC. The increase is mainly cause to scale-up the irradiation source (a 1000 W Xe lamp) as the E_{EO} values are given per m^3. That is why for the system to be sustainable it has to be solar driven.

In literature E_{EO} is the most reported figure-of-merit due to its suitability for low concentration range. Electrical energy per order has been calculated for different applications and using different photoelectrochemical processes. Bennani et al. [62] studied the influence of the radiation intensity on the E_{EO} and degradation of phenol. They estimated E_{EO}<4 kW h·m^{-3}·order^{-1} to reach conversions over 90% of phenol. However, using lower UV radiation intensities entailed more energy efficient processes despite the treatment time being higher. Collivignarelli, et al. [23] obtained E_{EO}=152 kW h·m^{-3}·order^{-1} for a decolorization process (based on EAP+H_2O_2), after 2 h of contact time and only taking into account the power necessary for the UV lamp and power supply. Bessegato et al. [63,64] estimated the electric energy per order for the mineralization of Benzophenone-3 (BP-3) in distilled water and hair dyeing wastewater using different combinations of Advanced Oxidation Processes (AOPs). Using O_3/EAP processes they reported E_{EO} of 20 kW h·m^{-3}·order^{-1} and ~150 kW h·m^{-3}·order^{-1} to achieve a mineralization of around 60 and 50% for the treatment of BP-3 and hair dye effluent, respectively. Lower E_{EO} and higher mineralization efficiencies could be achieved using O_3/UV/H_2O_2 systems. The E_{EO} was used to assess the performance of an annular photoelectrocatalytic reactor using multiple discs coated with TiO_2 on the electrochemically assisted photocatalytic degradation of a pharmaceutical (acetaminophen) [65]. The calculated E_{EO} values were 83 and 67 kW h·m^{-3}·order^{-1} at 4.0 and 8.0 V, respectively. Thus, the values for the EAP system studied here were lower to those reported in other articles [10] and could also be attributed to the application of a photoanode activated by solar light.

4. Conclusions

The performance of a EAP system based on WO_3 plate-like structures on the degradation of a mixture of CECs in simulated wastewater plant effluent was evaluated using two different cathodes, Pt and carbon gas diffusion electrode. The cell configuration, in which the photoanode was irradiated back-face through FTO glass and was facing the cathode, was suitable to degrade CECs in wastewater treatment plant effluent. Using carbon paper GDE as a cathode, without the need of flowing air, yielded higher degradation rates compared to Pt. Furthermore, the feasibility of the EAP system to work under visible radiation was proven, attaining high conversions of the different CECs. Moreover, this was also verified by the electrical energy per order, which was lower than 0.3 $kWh \cdot m^{-3} \cdot order^{-1}$ for each CEC considering solar irradiation conditions.

Despite several ROS being identified, such as $O_2^{\cdot-}$ or H_2O_2, photogenerated holes played the most important part in the CECs removal in SWWE. When carbon GDE was used, H_2O_2 was generated with Faradaic efficiencies near 55%. Thus, this EAP system may have potential for disinfection of water or to be coupled with other advanced oxidation processes which utilise H_2O_2, such as electro-Fenton or solar photoelectro-Fenton.

Acknowledgements

The authors wish to thank the EU-India H2020 cooperation program for funding this work under the PANIWATER project (RIA GA-820718). Álvaro Tolosana Moranchel also thank the Consejería de Educación, Juventud y Deporte of the Comunidad de Madrid for the Ayuda Destinada a la Atracción de Talento Investigador (2020-T2/AMB-19927) granted to him.

5. References

[1] N.H. Tran, M. Reinhard, K.Y.H. Gin, Occurrence and fate of emerging contaminants in municipal wastewater treatment plants from different geographical regions-a review, Water Res. 133 (2018) 182–207. https://doi.org/10.1016/J.WATRES.2017.12.029.

[2] M.K. Shahid, A. Kashif, A. Fuwad, Y. Choi, Current advances in treatment technologies for removal of emerging contaminants from water – A critical

review, Coord. Chem. Rev. 442 (2021) 213993. https://doi.org/10.1016/J.CCR.2021.213993.

[3] O.F.S. Khasawneh, P. Palaniandy, Occurrence and removal of pharmaceuticals in wastewater treatment plants, Process Saf. Environ. Prot. 150 (2021) 532–556. https://doi.org/10.1016/J.PSEP.2021.04.045.

[4] V. Rilstone, L. Vignale, J. Craddock, A. Cushing, Y. Filion, P. Champagne, The role of antibiotics and heavy metals on the development, promotion, and dissemination of antimicrobial resistance in drinking water biofilms, Chemosphere. 282 (2021) 131048. https://doi.org/10.1016/J.CHEMOSPHERE.2021.131048.

[5] R. Delli Compagni, M. Gabrielli, F. Polesel, A. Turolla, S. Trapp, L. Vezzaro, M. Antonelli, Risk assessment of contaminants of emerging concern in the context of wastewater reuse for irrigation: An integrated modelling approach, Chemosphere. 242 (2020) 125185. https://doi.org/10.1016/j.chemosphere.2019.125185.

[6] I. Sirés, E. Brillas, Remediation of water pollution caused by pharmaceutical residues based on electrochemical separation and degradation technologies: A review, Environ. Int. 40 (2012) 212–229. https://doi.org/10.1016/j.envint.2011.07.012.

[7] J. Byrne, P. Dunlop, J. Hamilton, P. Fernández-Ibáñez, I. Polo-López, P. Sharma, A. Vennard, A Review of Heterogeneous Photocatalysis for Water and Surface Disinfection, Molecules. 20 (2015) 5574–5615. https://doi.org/10.3390/molecules20045574.

[8] Y. Wang, M. Zu, X. Zhou, H. Lin, F. Peng, S. Zhang, Designing efficient TiO2-based photoelectrocatalysis systems for chemical engineering and sensing, Chem. Eng. J. 381 (2020) 122605. https://doi.org/10.1016/j.cej.2019.122605.

[9] M. Pelaez, N.T. Nolan, S.C. Pillai, M.K. Seery, P. Falaras, A.G. Kontos, P.S.M. Dunlop, J.W.J. Hamilton, J.A. Byrne, K. O'Shea, M.H. Entezari, D.D. Dionysiou, A review on the visible light active titanium dioxide photocatalysts for environmental applications, Appl. Catal. B Environ. 125 (2012) 331–349. https://doi.org/10.1016/J.APCATB.2012.05.036.

[10] E. Kusmierek, Semiconductor electrode materials applied in photoelectrocatalytic wastewater treatment—An overview, Catalysts. 10 (2020) 1–49. https://doi.org/10.3390/catal10040439.

[11] A. Tolosana-Moranchel, N. Pichel, H. Lubarsky, J.A. Byrne, P. Fernández-Ibañez, Photoelectrocatalytic degradation of pharmaceuticals and inactivation of viruses in water with tungsten oxide electrodes, J. Environ. Chem. Eng. 10 (2022) 107955. https://doi.org/10.1016/j.jece.2022.107955.

[12] K. Cho, S. Lee, H. Kim, H.E. Kim, A. Son, E. ju Kim, M. Li, Z. Qiang, S.W. Hong, Effects of reactive oxidants generation and capacitance on photoelectrochemical water disinfection with self-doped titanium dioxide nanotube arrays, Appl. Catal. B Environ. 257 (2019) 117910.

https://doi.org/10.1016/j.apcatb.2019.117910.

[13] L. Yu, Z. Wang, L. Shi, S. Yuan, Y. Zhao, J. Fang, W. Deng, Photoelectrocatalytic performance of TiO 2 nanoparticles incorporated TiO 2 nanotube arrays, Appl. Catal. B Environ. 113–114 (2012) 318–325. https://doi.org/10.1016/j.apcatb.2011.12.004.

[14] R.M. Fernández-Domene, R. Sánchez-Tovar, B. Lucas-granados, M.J. Muñoz-Portero, J. García-Antón, Elimination of pesticide atrazine by photoelectrocatalysis using a photoanode based on WO3 nanosheets, Chem. Eng. J. 350 (2018) 1114–1124. https://doi.org/10.1016/j.cej.2018.06.015.

[15] Y. Li, X. Wei, X. Yan, J. Cai, A. Zhou, M. Yang, K. Liu, Construction of inorganic-organic 2D/2D WO3/g-C3N4 nanosheet arrays toward efficient photoelectrochemical splitting of natural seawater, Phys. Chem. Chem. Phys. 18 (2016) 10255–10261. https://doi.org/10.1039/c6cp00353b.

[16] F.C. Moreira, R.A.R. Boaventura, E. Brillas, V.J.P. Vilar, Electrochemical advanced oxidation processes: A review on their application to synthetic and real wastewaters, Appl. Catal. B Environ. 202 (2017) 217–261. https://doi.org/10.1016/j.apcatb.2016.08.037.

[17] N.F.F. Moreira, C. Narciso-da-Rocha, M.I. Polo-López, L.M. Pastrana-Martínez, J.L. Faria, C.M. Manaia, P. Fernández-Ibáñez, O.C. Nunes, A.M.T. Silva, Solar treatment (H2O2, TiO2-P25 and GO-TiO2 photocatalysis, photo-Fenton) of organic micropollutants, human pathogen indicators, antibiotic resistant bacteria and related genes in urban wastewater, Water Res. 135 (2018) 195–206. https://doi.org/10.1016/j.watres.2018.01.064.

[18] I. Salmerón, P.K. Sharma, M.I. Polo-López, A. Tolosana, S. McMichael, I. Oller, J.A. Byrne, P. Fernández-Ibáñez, Electrochemically assisted photocatalysis for the simultaneous degradation of organic micro-contaminants and inactivation of microorganisms in water, Process Saf. Environ. Prot. 147 (2021) 488–496. https://doi.org/10.1016/j.psep.2020.09.060.

[19] L. Cheng, T. Jiang, J. Zhang, Photoelectrocatalytic degradation of deoxynivalenol on CuO-Cu2O/WO3 ternary film: Mechanism and reaction pathways, Sci. Total Environ. 776 (2021). https://doi.org/10.1016/j.scitotenv.2021.145840.

[20] H. Tang, Q. Shang, Y. Tang, X. Yi, Y. Wei, K. Yin, M. Liu, C. Liu, Static and continuous flow photoelectrocatalytic treatment of antibiotic wastewater over mesh of TiO2 nanotubes implanted with g-C3N4 nanosheets, J. Hazard. Mater. 384 (2020) 121248. https://doi.org/10.1016/J.JHAZMAT.2019.121248.

[21] C. Xue, D. Li, Y. Li, N. Li, F. Zhang, Y. Wang, Q. Chang, S. Hu, 3D-carbon dots decorated black TiO2 nanotube Array@Ti foam with enhanced photothermal and photocatalytic activities, Ceram. Int. 45 (2019) 17512–17520. https://doi.org/10.1016/j.ceramint.2019.05.313.

[22] G. Divyapriya, S. Singh, C.A. Martínez-huitle, J. Scaria, A. V Karim, P. V Nidheesh, Treatment of real wastewater by photoelectrochemical methods: An overview, Chemosphere. 276 (2021) 130188. https://doi.org/10.1016/j.chemosphere.2021.130188.

[23] M.C. Collivignarelli, A. Abbà, M. Carnevale Miino, H. Arab, M. Bestetti, S. Franz, Decolorization and biodegradability of a real pharmaceutical wastewater treated by H2O2-assisted photoelectrocatalysis on TiO2 meshes, J. Hazard. Mater. 387 (2020) 121668. https://doi.org/10.1016/j.jhazmat.2019.121668.

[24] P. Alulema-Pullupaxi, P.J. Espinoza-Montero, C. Sigcha-Pallo, R. Vargas, L. Fernández, J.M. Peralta-Hernández, J.L. Paz, Fundamentals and applications of photoelectrocatalysis as an efficient process to remove pollutants from water: A review, Chemosphere. 281 (2021) 130821. https://doi.org/10.1016/j.chemosphere.2021.130821.

[25] J. Bai, Y. Liu, J. Li, B. Zhou, Q. Zheng, W. Cai, A novel thin-layer photoelectrocatalytic (PEC) reactor with double-faced titania nanotube arrays electrode for effective degradation of tetracycline, Appl. Catal. B Environ. 98 (2010) 154–160. https://doi.org/10.1016/J.APCATB.2010.05.024.

[26] M. José Martín de Vidales, L. Mais, C. Sáez, P. Cañizares, F.C. Walsh, M.A. Rodrigo, C. de A. Rodrigues, C. Ponce de León, Photoelectrocatalytic Oxidation of Methyl Orange on a TiO2 Nanotubular Anode Using a Flow Cell, Chem. Eng. Technol. 39 (2016) 135–141. https://doi.org/10.1002/ceat.201500085.

[27] K. Li, H. Zhang, Y. He, T. Tang, D. Ying, Y. Wang, T. Sun, J. Jia, Novel wedge structured rotating disk photocatalytic reactor for post-treatment of actual textile wastewater, Chem. Eng. J. 268 (2015) 10–20. https://doi.org/10.1016/j.cej.2015.01.039.

[28] Y. Xu, Y. He, X. Cao, D. Zhong, J. Jia, TiO2/Ti rotating disk photoelectrocatalytic (PEC) reactor: A combination of highly effective thin-film PEC and conventional PEC processes on a single electrode, Environ. Sci. Technol. 42 (2008) 2612–2617. https://doi.org/10.1021/es702921h.

[29] A. Hankin, F.E. Bedoya-Lora, C.K. Ong, J.C. Alexander, F. Petter, G.H. Kelsall, From millimetres to metres: the critical role of current density distributions in photo-electrochemical reactor design, Energy Environ. Sci. 10 (2017) 346–360. https://doi.org/10.1039/C6EE03036J.

[30] M.I. Polo-López, I. García-Fernández, T. Velegraki, A. Katsoni, I. Oller, D. Mantzavinos, P. Fernández-Ibáñez, Mild solar photo-Fenton: An effective tool for the removal of Fusarium from simulated municipal effluents, Appl. Catal. B Environ. 111–112 (2012) 545–554. https://doi.org/10.1016/j.apcatb.2011.11.006.

[31] G. Maniakova, M.I. Polo-López, I. Oller, M.J. Abeledo-Lameiro, S. Malato, L. Rizzo, Simultaneous disinfection and microcontaminants elimination of urban wastewater secondary effluent by solar advanced oxidation sequential treatment at pilot scale, J. Hazard. Mater. 436 (2022) 2–10.

https://doi.org/10.1016/j.jhazmat.2022.129134.

[32] K.H. Rashid, A.A. Khadom, Sodium sulfite as an oxygen scavenger for the corrosion control of mild steel in petroleum refinery wastewater: optimization, mathematical modeling, surface morphology and reaction kinetics studies, React. Kinet. Mech. Catal. 129 (2020) 1027–1046. https://doi.org/10.1007/s11144-020-01738-3.

[33] S. McMichael, A. Tolosana-Moranchel, M.A.L.R.M. Cortes, J.W.J. Hamilton, P. Fernandez-Ibanez, J.A. Byrne, An investigation of photoelectrocatalytic disinfection of water using titania nanotube photoanodes with carbon cathodes and determination of the radicals produced, Appl. Catal. B Environ. 311 (2022) 121339. https://doi.org/10.1016/j.apcatb.2022.121339.

[34] R.J. Matson, K.A. Emery, R.E. Bird, Terrestrial solar spectra, solar simulation and solar cell short-circuit current calibration: A review, Sol. Cells. 11 (1984) 105–145. https://doi.org/10.1016/0379-6787(84)90022-X.

[35] A. Tolosana-Moranchel, A. Montejano, J.A. Casas, A. Bahamonde, Elucidation of the photocatalytic-mechanism of phenolic compounds, J. Environ. Chem. Eng. 6 (2018). https://doi.org/10.1016/j.jece.2018.08.068.

[36] B.R. Cruz-Ortiz, J.W.J. Hamilton, C. Pablos, L. Díaz-Jiménez, D.A. Cortés-Hernández, P.K. Sharma, M. Castro-Alférez, P. Fernández-Ibañez, P.S.M. Dunlop, J.A. Byrne, Mechanism of photocatalytic disinfection using titania-graphene composites under UV and visible irradiation, Chem. Eng. J. 316 (2017) 179–186. https://doi.org/10.1016/j.cej.2017.01.094.

[37] E. Torad, E.H. Ismail, M.M. Mohamed, M.M.H. Khalil, Tuning the redox potential of Ag@Ag2O/WO3 and Ag@Ag2S/WO3 photocatalysts toward diclofenac oxidation and nitrophenol reduction, Mater. Res. Bull. 137 (2021) 111193. https://doi.org/10.1016/j.materresbull.2020.111193.

[38] K.I. Ishibashi, A. Fujishima, T. Watanabe, K. Hashimoto, Detection of active oxidative species in TiO2 photocatalysis using the fluorescence technique, Electrochem. Commun. 2 (2000) 207–210. https://doi.org/10.1016/S1388-2481(00)00006-0.

[39] O. Fónagy, E. Szabó-Bárdos, O. Horváth, 1,4-Benzoquinone and 1,4-hydroquinone based determination of electron and superoxide radical formed in heterogeneous photocatalytic systems, J. Photochem. Photobiol. A Chem. 407 (2021) 113057. https://doi.org/10.1016/j.jphotochem.2020.113057.

[40] Y. Nosaka, A.Y. Nosaka, Generation and Detection of Reactive Oxygen Species in Photocatalysis, Chem. Rev. 117 (2017) 11302–11336. https://doi.org/10.1021/acs.chemrev.7b00161.

[41] G. Longobucco, L. Pasti, A. Molinari, N. Marchetti, S. Caramori, V. Cristino, R. Boaretto, C.A. Bignozzi, Photoelectrochemical mineralization of emerging contaminants at porous WO3 interfaces, Appl. Catal. B Environ. 204 (2017) 273–282.

https://doi.org/10.1016/j.apcatb.2016.11.007.

[42] A. Son, J. Lee, C. Lee, K. Cho, J. Lee, S.W. Hong, Persulfate enhanced photoelectrochemical oxidation of organic pollutants using self-doped TiO2nanotube arrays: Effect of operating parameters and water matrix, Water Res. 191 (2021). https://doi.org/10.1016/j.watres.2021.116803.

[43] C. Pablos, J. Marugán, C. Adán, M. Osuna, R. van Grieken, Performance of TiO2 photoanodes toward oxidation of methanol and E. coli inactivation in water in a scaled-up photoelectrocatalytic reactor, Electrochim. Acta. (2017). https://doi.org/10.1016/j.electacta.2017.11.103.

[44] E. Mousset, V. Huang Weiqi, B. Foong Yang Kai, J.S. Koh, J.W. Tng, Z. Wang, O. Lefebvre, A new 3D-printed photoelectrocatalytic reactor combining the benefits of a transparent electrode and the Fenton reaction for advanced wastewater treatment, J. Mater. Chem. A. 5 (2017) 24951–24964. https://doi.org/10.1039/c7ta08182k.

[45] C. Wang, Y. Xue, P. Wang, Y. Ao, Effects of water environmental factors on the photocatalytic degradation of sulfamethoxazole by AgI/UiO-66 composite under visible light irradiation, J. Alloys Compd. 748 (2018) 314–322. https://doi.org/10.1016/j.jallcom.2018.03.129.

[46] Y. fan Su, G.B. Wang, D.T.F. Kuo, M. ling Chang, Y. hsin Shih, Photoelectrocatalytic degradation of the antibiotic sulfamethoxazole using TiO2/Ti photoanode, Appl. Catal. B Environ. 186 (2016) 184–192. https://doi.org/10.1016/j.apcatb.2016.01.003.

[47] Q. Cai, J. Hu, Decomposition of sulfamethoxazole and trimethoprim by continuous UVA/LED/TiO2 photocatalysis: Decomposition pathways, residual antibacterial activity and toxicity, J. Hazard. Mater. 323 (2017) 527–536. https://doi.org/10.1016/j.jhazmat.2016.06.006.

[48] C. Lara-Pérez, E. Leyva, B. Zermeño, I. Osorio, C. Montalvo, E. Moctezuma, Photocatalytic degradation of diclofenac sodium salt: adsorption and reaction kinetic studies, Environ. Earth Sci. 79 (2020) 1–13. https://doi.org/10.1007/s12665-020-09017-z.

[49] H. Sudrajat, S. Babel, Role of reactive species in the photocatalytic degradation of amaranth by highly active N-doped WO3, Bull. Mater. Sci. 40 (2017) 1421–1428. https://doi.org/10.1007/s12034-017-1502-1.

[50] A.I. Navarro-Aguilar, S. Obregón, D. Sanchez-Martinez, D.B. Hernández-Uresti, An efficient and stable WO3/g-C3N4 photocatalyst for ciprofloxacin and orange G degradation, J. Photochem. Photobiol. A Chem. 384 (2019) 112010. https://doi.org/10.1016/J.JPHOTOCHEM.2019.112010.

[51] J.T. Schneider, D.S. Firak, R.R. Ribeiro, P. Peralta-Zamora, Use of scavenger agents in heterogeneous photocatalysis: truths, half-truths, and misinterpretations, Phys. Chem. Chem. Phys. 22 (2020) 15723–15733. https://doi.org/10.1039/d0cp02411b.

[52] H. Dong, Z. Qiang, X. Yuan, A. Luo, Effects of bromide and iodide on the chlorination of diclofenac: Accelerated chlorination and enhanced formation of disinfection by-products, Sep. Purif. Technol. 193 (2018)

415–420. https://doi.org/10.1016/J.SEPPUR.2017.09.068.

[53] A. Farhat, J. Keller, S. Tait, J. Radjenovic, Assessment of the impact of chloride on the formation of chlorinated by-products in the presence and absence of electrochemically activated sulfate, Chem. Eng. J. 330 (2017) 1265–1271. https://doi.org/10.1016/j.cej.2017.08.033.

[54] H. Gao, J. Chen, Y. Zhang, X. Zhou, Sulfate radicals induced degradation of Triclosan in thermally activated persulfate system, Chem. Eng. J. 306 (2016) 522–530. https://doi.org/10.1016/j.cej.2016.07.080.

[55] E. Brillas, C.A. Martínez-Huitle, Decontamination of wastewaters containing synthetic organic dyes by electrochemical methods. An updated review, Appl. Catal. B Environ. 166–167 (2015) 603–643. https://doi.org/10.1016/j.apcatb.2014.11.016.

[56] W.H. Organization, Guidelines for drinking-water quality: first addendum to the fourth edition, (2017).

[57] R. Daghrir, P. Drogui, M.A. El Khakani, Photoelectrocatalytic oxidation of chlortetracycline using Ti/TiO 2 photo-anode with simultaneous H2O2 production, Electrochim. Acta. 87 (2013) 18–31. https://doi.org/10.1016/j.electacta.2012.09.020.

[58] F. Yu, M. Zhou, X. Yu, Cost-effective electro-Fenton using modified graphite felt that dramatically enhanced on H2O2 electro-generation without external aeration, Electrochim. Acta. 163 (2015) 182–189. https://doi.org/10.1016/J.ELECTACTA.2015.02.166.

[59] W. Zhou, L. Rajic, L. Chen, K. Kou, Y. Ding, X. Meng, Y. Wang, B. Mulaw, J. Gao, Y. Qin, A.N. Alshawabkeh, Activated carbon as effective cathode material in iron-free Electro-Fenton process: Integrated H2O2 electrogeneration, activation, and pollutants adsorption, Electrochim. Acta. 296 (2019) 317–326. https://doi.org/10.1016/J.ELECTACTA.2018.11.052.

[60] Y. Song, G.R. Buettner, Thermodynamic and kinetic considerations for the reaction of semiquinone radicals to form superoxide and hydrogen peroxide, Free Radic. Biol. Med. 49 (2010) 919–962. https://doi.org/10.1016/J.FREERADBIOMED.2010.05.009.

[61] J.R. Bolton, K.G. Bircher, W. Tumas, C.A. Tolman, Figures-of-merit for the technical development and application of advanced oxidation technologies for both electric- and solar-driven systems, Pure Appl. Chem. 73 (2001) 627–637. https://doi.org/10.1351/pac200173040627.

[62] Y. Bennani, P. Appel, L.C. Rietveld, Optimisation of parameters in a solar light-induced photoelectrocatalytic process with a TiO2/Ti composite electrode prepared by paint-thermal decomposition, J. Photochem. Photobiol. A Chem. 305 (2015) 83–92. https://doi.org/10.1016/j.jphotochem.2015.03.009.

[63] J.Y.U. Kim, G.G. Bessegato, B.C. de Souza, J.J. da Silva, M.V.B. Zanoni, Efficient treatment of swimming pool water by photoelectrocatalytic ozonation: Inactivation of Candida parapsilosis and mineralization of

Benzophenone-3 and urea, Chem. Eng. J. 378 (2019) 122094. https://doi.org/10.1016/j.cej.2019.122094.

[64] G.G. Bessegato, J.C. De Souza, J.C. Cardoso, M.V.B. Zanoni, Assessment of several advanced oxidation processes applied in the treatment of environmental concern constituents from a real hair dye wastewater, J. Environ. Chem. Eng. 6 (2018) 2794–2802. https://doi.org/10.1016/j.jece.2018.04.041.

[65] R. Montenegro-Ayo, J.C. Morales-Gomero, H. Alarcon, S. Cotillas, P. Westerhoff, S. Garcia-Segura, Scaling up Photoelectrocatalytic Reactors: A TiO2 Nanotube-Coated Disc Compound Reactor Effectively Degrades Acetaminophen, Water. 11 (2019) 2522. https://doi.org/10.3390/w11122522.